Research Article | Vol. 25, No. 9 | 1 May 2017 | OPTICS EXPRESS 9634
Optics EXPRESS

Simultaneous wavelength and orbital angular momentum demultiplexing using tunable MEMS-based Fabry-Perot filter

VLADIMIR S. LYUBOPYTOV,[1,2] ALEXEY P. PORFIREV,[3,4] STANISLAV O. GURBATOV,[5,6] SUJOY PAUL,[1] MARTIN F. SCHUMANN,[7,8] JULIJAN CESAR,[1] MOHAMMADREZA MALEKIZANDI,[1] MOHAMMAD T. HAIDAR,[1] MARTIN WEGENER,[7,8] ARKADI CHIPOULINE,[1,*] AND FRANKO KÜPPERS[1,9]

[1]*Institute for Microwave Engineering and Photonics, Technische Universität Darmstadt, Merckstr. 25, 64283 Darmstadt, Germany*
[2]*Department of Photonics Engineering, Technical University of Denmark (DTU), Ørsteds Plads 343, 2800 Kgs. Lyngby, Denmark*
[3]*Samara National Research University, Moskovskoye shosse 34, Samara 443086, Russia*
[4]*Image Processing Systems Institute - Branch of the Federal Scientific Research Centre "Crystallography and Photonics" of Russian Academy of Sciences, Molodogvardejskaya St. 151, Samara 443001, Russia*
[5]*Far Eastern Federal University, 8 Sukhanova Str., Vladivostok 690041, Russia*
[6]*Institute of Automation and Control Processes, Far Eastern Branch of the Russian Academy of Sciences (IACP FEB RAS), Radio Str. 5, Vladivostok 690041, Russia*
[7]*Institute of Nanotechnology, Karlsruhe Institute of Technology (KIT), 76021 Karlsruhe, Germany*
[8]*Institute of Applied Physics, Karlsruhe Institute of Technology (KIT), 76128 Karlsruhe, Germany*
[9]*College of Optical Sciences, University of Arizona, 1630 E. University Blvd., Tucson, Arizona 85721, USA*
**chipouline@imp.tu-darmstadt.de*

Abstract: In this paper, we experimentally demonstrate simultaneous wavelength and orbital angular momentum (OAM) multiplexing/demultiplexing of 10 Gbit/s data streams using a new on-chip micro-component – tunable MEMS-based Fabry-Perot filter integrated with a spiral phase plate. In the experiment, two wavelengths, each of them carrying two channels with zero and nonzero OAMs, form four independent information channels. In case of spacing between wavelength channels of 0.8 nm and intensity modulation, power penalties relative to the transmission of one channel do not exceed 1.45, 0.79 and 0.46 dB at the hard-decision forward-error correction (HD-FEC) bit-error-rate (BER) limit 3.8×10^{-3} when multiplexing a Gaussian beam and OAM beams of azimuthal orders 1, 2 and 3 respectively. In case of phase modulation, power penalties do not exceed 1.77, 0.54 and 0.79 dB respectively. At the 0.4 nm wavelength grid, maximum power penalties at the HD-FEC BER threshold relative to the 0.8 nm wavelength spacing read 0.83, 0.84 and 1.15 dB when multiplexing a Gaussian beam and OAM beams of 1st, 2nd and 3rd orders respectively. The novelty and impact of the proposed filter design is in providing practical, integrable, cheap, and reliable transformation of OAM states simultaneously with the selection of a particular wavelength in wavelength division multiplexing (WDM). The proposed on-chip device can be useful in future high-capacity optical communications with spatial- and wavelength-division multiplexing, especially for short-range communication links and optical interconnects.

© 2017 Optical Society of America

OCIS codes: (120.2230) Fabry-Perot; (130.7408) Wavelength filtering devices; (230.4685) Optical microelectromechanical devices; (050.4865) Optical vortices.

References and links

1. I. Djordjevic, W. Ryan, and B. Vasic, *Coding for Optical Channels* (Springer Verlag, 2010), Chap. 10.

#282884 https://doi.org/10.1364/OE.25.009634
Journal © 2017 Received 14 Dec 2016; revised 14 Mar 2017; accepted 17 Mar 2017; published 19 Apr 2017
Corrected: 15 May 2017

Optics EXPRESS

2. R.-J. Essiambre, G. Kramer, P. J. Winzer, G. J. Foschini, and B. Goebel, "Capacity limits of optical fiber networks," J. Lightwave Technol. **28**(4), 662–701 (2010).
3. A. D. Ellis, N. Mac Suibhne, D. Saad, and D. N. Payne, "Communication networks beyond the capacity crunch," Philos Trans A Math Phys Eng Sci **374**(2062), 20150191 (2016).
4. D. J. Richardson, "New optical fibres for high-capacity optical communications," Philos Trans A Math Phys Eng Sci **374**(2062), 20140441 (2016).
5. D. J. Richardson, J. M. Fini, and L. E. Nelson, "Space-division multiplexing in optical fiber," Nat. Photonics **7**(5), 354–362 (2013).
6. N. Zhao, X. Li, G. Li, and J. M. Kahn, "Capacity limit of spatially multiplexed free-space communication," Nat. Photonics **9**(12), 822–826 (2015).
7. J. Wang, M. J. Padgett, S. Ramachandran, M. P. J. Lavery, H. Huang, Y. Yue, N. Bozinovic, S. E. Golowich, and A. E. Willner, "Multimode communications using orbital angular momentum," in *Optical Fiber Telecommunications VIB: Systems and Networks*, I. P. Kaminow, T. Li, and A. E. Willner, ed. (Academic, 2013).
8. A. E. Willner, H. Huang, Y. Yan, Y. Ren, N. Ahmed, G. Xie, C. Bao, L. Li, Y. Cao, Z. Zhao, J. Wang, M. P. J. Lavery, M. Tur, S. Ramachandran, A. F. Molisch, N. Ashrafi, and S. Ashrafi, "Optical communications using orbital angular momentum beams," Adv. Opt. Photonics **7**(1), 66–106 (2015).
9. L. Allen, M. W. Beijersbergen, R. J. Spreeuw, and J. P. Woerdman, "Orbital angular momentum of light and the transformation of Laguerre-Gaussian laser modes," Phys. Rev. A **45**(11), 8185–8189 (1992).
10. S. Berdagué and P. Facq, "Mode division multiplexing in optical fibers," Appl. Opt. **21**(11), 1950–1955 (1982).
11. A. Li, A. Al Amin, X. Chen, and W. Shieh, "Transmission of 107-Gb/s mode and polarization multiplexed CO-OFDM signal over a two-mode fiber," Opt. Express **19**(9), 8808–8814 (2011).
12. C. Koebele, M. Salsi, D. Sperti, P. Tran, P. Brindel, H. Mardoyan, S. Bigo, A. Boutin, F. Verluise, P. Sillard, M. Astruc, L. Provost, F. Cerou, and G. Charlet, "Two mode transmission at 2×100 Gb/s, over 40 km-long prototype few-mode fiber, using LCOS-based programmable mode multiplexer and demultiplexer," Opt. Express **19**(17), 16593–16600 (2011).
13. R. Ryf, S. Randel, A. H. Gnauck, C. Bolle, A. Sierra, S. Mumtaz, M. Esmaeelpour, E. C. Burrows, R.-J. Essiambre, P. J. Winzer, D. W. Peckham, A. H. McCurdy, and R. Lingle, Jr., "Mode-division multiplexing over 96 km of few-mode fiber using coherent 6x6 MIMO processing," J. Lightwave Technol. **30**(4), 521–531 (2012).
14. G. Gibson, J. Courtial, M. Padgett, M. Vasnetsov, V. Pas'ko, S. Barnett, and S. Franke-Arnold, "Free-space information transfer using light beams carrying orbital angular momentum," Opt. Express **12**(22), 5448–5456 (2004).
15. P. Boffi, P. Martelli, A. Gatto, and M. Martinelli, "Mode-division multiplexing in fibre-optic communications based on orbital angular momentum," J. Opt. **15**(7), 075403 (2013).
16. N. Bozinovic, Y. Yue, Y. Ren, M. Tur, P. Kristensen, H. Huang, A. E. Willner, and S. Ramachandran, "Terabit-scale orbital angular momentum mode division multiplexing in fibers," Science **340**(6140), 1545–1548 (2013).
17. J. Carpenter, B. C. Thomsen, and T. D. Wilkinson, "Optical vortex based Mode Division Multiplexing over graded-index multimode fiber," in *Optical Fiber Communication Conference*, OSA Technical Digest (Optical Society of America, 2013), paper OTh4G.3.
18. H. Huang, G. Milione, M. P. J. Lavery, G. Xie, Y. Ren, Y. Cao, N. Ahmed, T. An Nguyen, D. A. Nolan, M.-J. Li, M. Tur, R. R. Alfano, and A. E. Willner, "Mode division multiplexing using an orbital angular momentum mode sorter and MIMO-DSP over a graded-index few-mode optical fibre," Sci. Rep. **5**, 14931 (2015).
19. A. Wang, L. Zhu, J. Liu, C. Du, Q. Mo, and J. Wang, "Demonstration of hybrid orbital angular momentum multiplexing and time-division multiplexing passive optical network," Opt. Express **23**(23), 29457–29466 (2015).
20. I. M. Fazal, N. Ahmed, J. Wang, J.-Y. Yang, Y. Yan, B. Shamee, H. Huang, Y. Yue, S. Dolinar, M. Tur, and A. E. Willner, "2 Tbit/s free-space data transmission on two orthogonal orbital-angular-momentum beams each carrying 25 WDM channels," Opt. Lett. **37**(22), 4753–4755 (2012).
21. J. Wang, J.-Y. Yang, I. M. Fazal, N. Ahmed, Y. Yan, H. Huang, Y. Ren, Y. Yue, S. Dolinar, M. Tur, and A. E. Willner, "Terabit free-space data transmission employing orbital angular momentum multiplexing," Nat. Photonics **6**(7), 488–496 (2012).
22. H. Huang, G. Xie, Y. Yan, N. Ahmed, Y. Ren, Y. Yue, D. Rogawski, M. J. Willner, B. I. Erkmen, K. M. Birnbaum, S. J. Dolinar, M. P. Lavery, M. J. Padgett, M. Tur, and A. E. Willner, "100 Tbit/s free-space data link enabled by three-dimensional multiplexing of orbital angular momentum, polarization, and wavelength," Opt. Lett. **39**(2), 197–200 (2014).
23. N. Ahmed, Z. Zhao, L. Li, H. Huang, M. P. J. Lavery, P. Liao, Y. Yan, Z. Wang, G. Xie, Y. Ren, A. Almaiman, A. J. Willner, S. Ashrafi, A. F. Molisch, M. Tur, and A. E. Willner, "Mode-division-multiplexing of multiple Bessel-Gaussian beams carrying orbital-angular-momentum for obstruction-tolerant free-space optical and millimetre-wave communication links," Sci. Rep. **6**(1), 22082 (2016).
24. S. N. Khonina, V. V. Kotlyar, R. V. Skidanov, V. A. Soifer, P. Laakkonen, and J. Turunen, "Gauss–Laguerre modes with different indices in prescribed diffraction orders of a diffractive phase element," Opt. Commun. **175**(4–6), 301–308 (2000).
25. G. C. G. Berkhout, M. P. J. Lavery, J. Courtial, M. W. Beijersbergen, and M. J. Padgett, "Efficient sorting of orbital angular momentum states of light," Phys. Rev. Lett. **105**(15), 153601 (2010).

Optics EXPRESS

26. X. Cai, J. Wang, M. J. Strain, B. Johnson-Morris, J. Zhu, M. Sorel, J. L. O'Brien, M. G. Thompson, and S. Yu, "Integrated compact optical vortex beam emitters," Science **338**(6105), 363–366 (2012).
27. H. Li, D. B. Phillips, X. Wang, Y.-L. D. Ho, L. Chen, X. Zhou, J. Zhu, S. Yu, and X. Cai, "Orbital angular momentum vertical-cavity surface-emitting lasers," Optica **2**(6), 547–552 (2015).
28. N. K. Fontaine, C. R. Doerr, and L. Buhl, "Efficient multiplexing and demultiplexing of free-space orbital angular momentum using photonic integrated circuits," in *Optical Fiber Communication Conference*, OSA Technical Digest (Optical Society of America, 2012), paper OTu1I.2.
29. T. Su, R. P. Scott, S. S. Djordjevic, N. K. Fontaine, D. J. Geisler, X. Cai, and S. J. B. Yoo, "Demonstration of free space coherent optical communication using integrated silicon photonic orbital angular momentum devices," Opt. Express **20**(9), 9396–9402 (2012).
30. L.-W. Luo, N. Ophir, C. P. Chen, L. H. Gabrielli, C. B. Poitras, K. Bergmen, and M. Lipson, "WDM-compatible mode-division multiplexing on a silicon chip," Nat. Commun. **5**, 3069 (2014).
31. Y. Li, X. Li, L. Chen, M. Pu, J. Jin, M. Hong, and X. Luo, "Orbital angular momentum multiplexing and demultiplexing by a single metasurface," Adv. Opt. Mater. **5**(2), 1600502 (2017).
32. S. Gringeri, B. Basch, V. Shukla, R. Egorov, and T. J. Xia, "Flexible architectures for optical transport nodes and networks," IEEE Commun. Mag. **48**(7), 40–50 (2010).
33. S. Gringeri, N. Bitar, and T. J. Xia, "Extending software defined network principles to include optical transport," IEEE Commun. Mag. **51**(3), 32–40 (2013).
34. S. Paul, V. S. Lyubopytov, M. F. Schumann, J. Cesar, A. Chipouline, M. Wegener, and F. Küppers, "Wavelength-selective orbital-angular-momentum beam generation using MEMS tunable Fabry-Perot filter," Opt. Lett. **41**(14), 3249–3252 (2016).
35. M. Ruffini, F. Slyne, C. Bluemm, N. Kitsuwan, and S. McGettrick, "Software defined networking for next generation converged metro-access networks," Opt. Fiber Technol. **26**, 31–41 (2015).
36. W. Zhang, H. Wang, and K. Bergman, "Next-generation optically interconnected high-performance data centers," J. Lightwave Technol. **30**(24), 3836–3844 (2012).
37. M. A. Taubenblatt, "Optical interconnects for high-performance computing," J. Lightwave Technol. **30**(4), 448–457 (2012).
38. S. Paul, C. Gierl, J. Cesar, M. Malekizandi, C. Neumeyr, M. Ortsiefer, F. Küppers, and Q. T. Le, "10-Gb/s direct modulation of widely tunable 1550-nm MEMS VCSEL," IEEE J. Sel. Top. Quantum Electron. **21**(6), 436–443 (2015).
39. H. Huang, Y. Ren, N. Ahmed, Y. Yan, Y. Yue, A. Bozovich, J.-Y. Yang, K. Birnbaum, J. Choi, B. Erkmen, S. Dolinar, M. Tur, and A. Willner, "Demonstration of OAM mode distortions monitoring using interference-based phase reconstruction," in *Conference on Lasers and Electro-Optics* (CLEO), OSA Technical Digest (online) (Optical Society of America, 2012), paper CF3C.4.
40. E. Yao, S. Franke-Arnold, J. Courtial, S. Barnett, and M. Padgett, "Fourier relationship between angular position and optical orbital angular momentum," Opt. Express **14**(20), 9071–9076 (2006).
41. "IEEE standard for Ethernet – amendment 3: physical layer specifications and management parameters for 40 Gb/s and 100 Gb/s operation over fiber optic cables," IEEE Std 802.3bm-2015 (2015).
42. J. Petrilla, "100G SR4 & RS (528, 514, 7, 10) FEC," Avago Technologies, Tech. Rep., September 2012. Available on http://www.ieee802.org/3/bm/public/sep12/petrilla_02a_0912_optx.pdf
43. "Spectral grids for WDM applications: DWDM frequency grid," Rec. ITU-T G.694.1 (ITU-T, 02/2012).

1. Introduction

The capacity of optical communication systems based on the existing multiplexing techniques in the time and frequency domains is often restricted by the nonlinear Shannon limit for single-mode transmission [1,2]. As a result, bandwidth of the optical communication proves to be insufficient to satisfy the exponentially growing demands for data transfer in the foreseeable future [3,4]. One of the considered ways to prevent the impending "capacity crunch" is the employment of spatial degree of freedom for multiplexing information channels in addition to the conventionally used time, wavelength and polarization domains. Spatial Division Multiplexing (SDM) [5,6] can be realized in free space or multimode optical fibers by using the basis of orthogonal modes. One of the possible sets of orthogonal modes can be one of the modes carrying orbital angular momentum (OAM) [7,8], which are characterized by the phase front vorticity of electromagnetic wave. It was recognized by Allen et al. [9] that a helically-phased light beam containing the azimuthal phase term $\exp(il\varphi)$, inherently possesses OAM of $l\hbar$ per photon, where integer l is the topological charge, φ is the azimuthal angle, and $\hbar$ is the Planck constant. Such a beam is commonly referred to as an optical vortex. Since optical vortices, carrying distinct OAM, form a basis of orthogonal functions, their applicability as independent signal carriers allows for SDM of the capacity of optical communication links. In other words, OAM-multiplexing can be treated as

Optics EXPRESS

a special case of Mode Division Multiplexing (MDM) [10–13], where the modal basis is represented by optical vortices [14–19].

Currently, a number of successful implementations of OAM-multiplexed transmission over relevant distances have been demonstrated in both optical fibers [16–19] and free space [20–23]. Usually, for generation and (de)multiplexing of optical vortices liquid crystal spatial light modulators (SLMs) [16,17,19–23] or separate spatial phase plates (SPPs) [14] are utilized. However, effective involvement of OAM-based transmission techniques into industrial applications requires robustness and repeatability, which is difficult to achieve with discrete components. Thus, development of compact, capable of mass production and on-chip integration optical components, providing the functionality for processing OAM-carrying signals, is desirable for robust and cost-effective OAM-based communications.

Significant attention of research groups has been focused on developing integrated devices for generation and (de)multiplexing of OAM modes. In [24,25] effective methods for demultiplexing OAM states has been suggested based on static optical elements, suitable for micro systems. Simple and robust silicon-integrated optical vortex emitters, capable of large-scale integration, have been proposed in [26]. Direct generation of OAM-beams has been demonstrated using a single-mode 860 nm vertical-cavity surface-emitting laser (VCSEL) with the dielectric SPP deposited on its top mirror [27]. A CMOS-compatible photonic integrated circuit (PIC) OAM-(de)multiplexer have been proposed in [28], and in [29] data transmission using the proposed PIC was experimentally demonstrated for two multiplexed OAM states.

On the other hand, introducing of new techniques should lean upon the achievements of matured, commercially successful techniques. Even though the OAM provides a theoretically infinite range of discrete states $l\hbar$, practically the efficiency of their excitation decreases with increasing l. Thus, to multiply the capacity of current optical communications, OAM-multiplexing should be superimposed over the wavelength-division multiplexing (WDM) technique. As in this case at each receiver in a broadcast network or at multiplexers in a switched network WDM-demultiplexing has to be applied to a demultiplexed OAM-channel (or vice versa), integration of wavelength- and OAM-demultiplexing functions in the same device is advantageous regarding miniaturization and minimization of losses. The problem of simultaneous selection of different wavelengths and spatial modes for the first time, to the best of our knowledge, was addressed in the work [30], were authors demonstrated WDM-compatible MDM with microring-based PIC for on-chip ultrahigh bandwidth communications. In [31], as an extension of the spatial modes separation method proposed in [24], the concept of simultaneous OAM, wavelength and polarization (de)multiplexing using a metasurface is proposed and simulated. At the same time, wide spectral tunability of a filter is desirable for colorless (de)multiplexing [32,33] in hybrid wavelength- and OAM-multiplexed optical networks.

In our paper [34] we have suggested a construction of widely wavelength-tunable MEMS-based Fabry-Perot filter with the micro-sized SPP deposited on the filter aperture. This device is capable of functioning simultaneously in both wavelength and OAM domains in 1550 nm telecom wavelength range: it simultaneously separates wavelengths in a tunable fashion, while providing the output beam with a fixed OAM defined by the topological charge of SPP. Fabrication of MEMS filters utilizes surface micromachining technology, suitable for mass fabrication in 2D arrays. Thus, by integrating filters with mass-manufacturable SPPs, high-purity OAM modes and their superposition states could be generated while maintaining advantages in cost and power efficiency.

In this paper we demonstrate the functionality of the proposed vortex MEMS filters to select simultaneously WDM and OAM channels. We consider this compact, on-chip integrable device to be especially useful for communication applications, where the distances are relatively short but high data rates are desirable, such as metro-access networks [19,35] and optical interconnects for data centers [36,37].

Optics EXPRESS

The paper is organized as follows. In Section 2 a brief description of the construction and main physical characteristics of the vortex MEMS filters are provided. Section 3 describes the experimental setup for simultaneous wavelength and OAM demultiplexing of data streams. In Section 4 the measurement scenarios used for penalty determination are considered and the obtained experimental results on the BER performance are demonstrated and discussed. Section 5 summarizes the results of this work.

2. Device structure and fabrication

A wavelength-tunable vortex MEMS filter is basically a Fabry-Perot MEMS resonator with an integrated SPP, as shown in Fig. 1(a). For an elaborated description of the structure and fabrication of the MEMS mirror, the readers are referred to [34,38]. A fully fabricated device comprises an anti-reflection coating (ARC), a Si substrate, a fixed bottom distributed Bragg reflector (DBR), a variable air-gap, a movable MEMS DBR and a SPP. First, a SiON ARC of $\lambda_0/4$ (λ_0 being the target center wavelength) thickness is deposited in a low-temperature (<80 °C) plasma enhanced chemical vapor deposition (PECVD) chamber. The bottom DBR comprising nine pairs of SiO_x/SiN_y dielectric layers in an alternating sequence are deposited on the other side of the wafer. To incorporate ~5 µm of air-gap, a Ni sacrificial layer is sputtered and laterally structured with lithography and wet-chemical etching. Then the layers of the MEMS DBR are deposited with the same material sequence. However, an intrinsic stress gradient is incorporated intentionally in the MEMS dielectric materials for the membrane to bend concavely after the sacrificial layer is completely removed. Each DBR layer has an optical thickness of $\lambda_0/4$, resulting in a total thickness of 5.5 µm. With a refractive index difference between SiO_x and SiN_y of $\Delta n = 0.5$, the MEMS mirror exhibits a reflectivity >99.5% over a broadband wavelength range of 120 nm around the center wavelength of 1550 nm. On top of the MEMS DBR a Cr/Au actuation electrode is evaporated. To accommodate the SPP, a circular opening in the Cr/Au layer is structured. Afterwards, the top DBR is covered with a Ni etch mask and dry etched to achieve the characteristic shape. Finally, both sacrificial layer and the etch mask are wet etched and the device is dried using a critical point drier. The resonant wavelength can be tuned either by electro-thermal actuation of the MEMS or just by changing the substrate temperature. As the suspension beams of the MEMS are fixed to fixed DBR surface, it can expand only in upward direction. Thus the optical cavity length is increased, resulting in a red-shift in the resonance wavelength. In contrast, a blue-shift of emission is prominent in thermal tuning scheme due to a slower thermal expansion of the MEMS compared to the Si substrate.

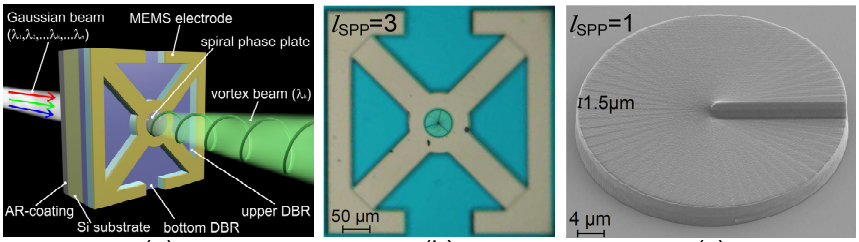

Fig. 1. (a) Scheme of a vortex MEMS Fabry-Perot filter. (b) Top view of a MEMS tunable Fabry-Perot filter with an integrated SPP of azimuthal order $l_{SPP} = 3$. (c) SEM image of a SPP of order $l_{SPP} = 1$ on a plane Si substrate.

An l-fold SPP is then printed on the aperture of the MEMS DBR. The estimated height, h_{SPP}, of the SPP depends on the azimuthal angle φ according to

$$h_{SPP}(\varphi) = \frac{\varphi l_{SPP} \lambda_0}{2\pi(n_{SPP} - n_0)}, \quad (1)$$

Optics EXPRESS

where l_{SPP} is the required topological charge of the phase plate, and n_{SPP} and n_0 are the refractive indices of the material of the SPP and the surrounding medium (in this case it is air), respectively. The SPP is fabricated utilizing direct laser writing of polymers (Photonic Professional GT with IP-Dip photoresist, nanoscribe GmbH, Germany) in a dip-in configuration to enable the integration directly on the surface of the finished MEMS device. While the design height depends continuously on φ, the mask is divided into 60 discrete steps – see Fig. 1(c). Consequently, the geometry can be sliced into layers of equal height which can be exposed one after another using the rapid galvo-scanning technique. Fabrication of a 52 µm-diameter SPP takes only approximately five minutes.

Figure 2 shows filter transmittance of the resonance wavelength when the filter is tuned using the electro-thermal actuation scheme. As can be seen, with an increasing MEMS current I_{MEMS}, the spectrum is red-shifted. The shape of the envelope follows the trace of the semiconductor optical amplifier (SOA). The MEMS-filter shows a full-width at half-maximum (FWHM) bandwidth of 0.2 nm and a free spectral range (FSR) of 126 nm. The FSR, defined by the spectral spacing between two consecutive modes, is one of the limiting factors (the other is the reflectivity bandwidth of the DBRs) for a mode-hop free tuning. It can be altered by designing an optimum air-gap by changing the stress gradient of the top DBR and reflectivity of the DBR layers. The bandwidth of the MEMS-filter does not change after integrating the SPP mask on its upper DBR. As we have shown in [34], MEMS filters with SPPs show only slight extra losses at the resonance wavelength compared to the MEMS filter without SPP. This difference, reliably measured for the filter with $l_{SPP} = 1$, amounts to 1.93 dB and can be explained by the additional absorption and scattering of the light by the SPP itself.

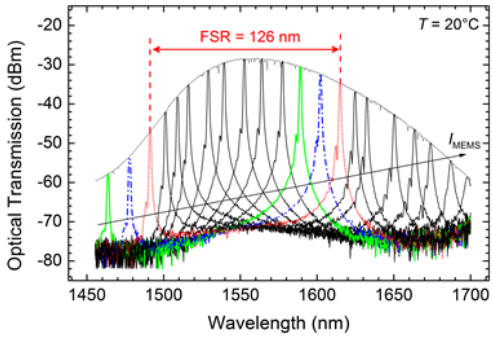

Fig. 2. Dependence of MEMS-filter transmittance of the resonance wavelength.

Figure 3 shows experimentally measured phase distributions at the output of vortex MEMS-filters of different azimuthal orders ($l_{SPP} = 1, 2, 3$), captured using the method proposed in [39] for three different wavelengths when the Gaussian beam is incident to the filter input. The OAM spectra of generated vortex beams (see [40]) calculated from the phase profiles show OAM-state purity not lower than 93.5, 93.3 and 92.3% for the SPPs of azimuthal orders $l_{SPP} = 1$, 2 and 3 respectively while the MEMS-filters are tuned across a wavelength range of more than 30 nm [34].

Optics EXPRESS

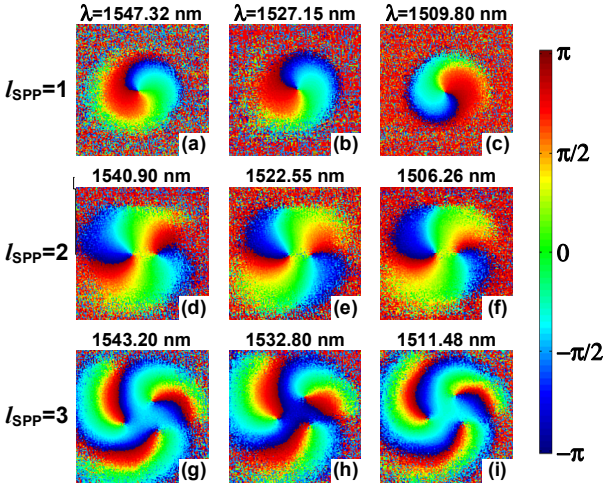

Fig. 3. Phase profiles for the main resonance mode of the vortex MEMS filters with SPPs of azimuthal orders l_{SPP} = 1, 2, 3 at different resonance wavelengths.

In order to reduce the complexity of experimental setup, in this work, as well as in [34], the thermal heating approach is applied for filter tuning, which allows smaller tuning range compared with the case of electro-thermal MEMS actuation. However, even with this simple approach the tuning range of more than 30 nm can be achieved. In [34] we have demonstrated 40 nm tuning range (from 1507.8 to 1547.8 nm) of the MEMS filter with almost linear dependence of resonance wavelength on the wafer temperature (changing from 16.5 to 29°C respectively).

3. Experimental setup

To perform wavelength- and OAM-multiplexed transmission tests, a prototype of an optical communication system was assembled, consisting of a typical fiber optic transmitter with a WDM multiplexer (WDM-MUX), free-space OAM multiplexer (OAM-MUX), and receiver, where simultaneous demultiplexing of wavelength and spatial channels is provided by the MEMS-filter – see Fig. 4. Two tunable external cavity lasers (ECLs) feed WDM-MUX generating two information channels with a variable wavelength difference. One of the wavelength channels is considered as primary, i.e. carrying the useful signal to be received, while another one is considered as secondary, i.e. carrying another signal, which performs as a disturbance. BER measurements have been performed with the primary channel only.

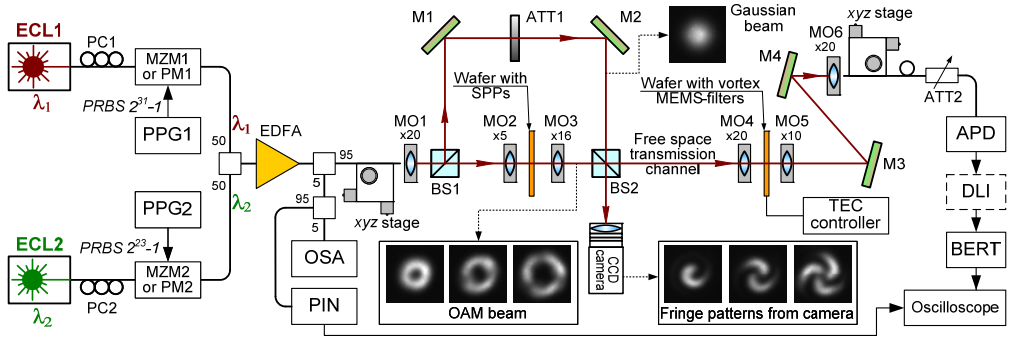

Fig. 4. Scheme of the experimental setup for the BER measurements.

After passing polarization controllers PC1 and PC2, the laser signals are independently modulated by Mach-Zehnder modulators (MZMs) or phase modulators (PMs) in case of

Optics EXPRESS

intensity or phase modulation, respectively. The modulators are driven by pseudorandom bit sequences (PRBS) of lengths of 2^{31}–1 and 2^{23}–1bits at 10 Gbit/s electrical signals, respectively. Modulators MZM1 and MZM2 provide extinction ratios of 9.2 and 9.46 dB, respectively. Being combined by a 50/50 coupler and pre-amplified using an erbium-doped fiber amplifier (EDFA), 95% of the WDM signal are coupled to the input of OAM-MUX. Another 5%-part of the generated WDM signal is split between the p-i-n photodiode (PIN) (95%) and optical spectrum analyzer (OSA) (5%). By connecting the digitizing oscilloscope to the output of PIN, initial eye-diagrams of individual WDM channels can be captured in order to optimize performance. OSA serves to monitor the spectrum of the generated WDM signals in order to ensure that WDM channels have equal powers and are separated with a certain $\Delta\lambda$. The total output power of EDFA is kept at the level of 20 dBm. Purposely no optical band-pass filter is used after EDFA for filtering amplified spontaneous emission (ASE), as it is to be filtered by the MEMS-filter.

Pre-amplified optical signal, collimated from the fiber output by microscope objective MO1, is split by the beam splitter BS1 to generate two copies of the WDM signal. Then one signal copy, being passed through SPP, acquires the OAM corresponding to the azimuthal order of SPP, whereas another one remains Gaussian. SPPs at the transmitter have the same construction as SPPs deposited on the apertures of MEMS filters, but are deposited directly on the Si substrate – see Fig. 1(c). The input beam is incident to SPP from the side of substrate, where an ARC is applied. Microscope objective MO2 serves to match the beam waist with the SPP, and MO3 collimates the output vortex beam. A path difference of ~35 cm between Gaussian beam and vortex beam provides ~1.17 ns delay between OAM-multiplexed channels. Beam splitter BS2 provides multiplexing of Gaussian and OAM beams, forming four independent information channels. Variable attenuator ATT1 allows for adjusting the ratio between powers transmitted in Gaussian and OAM channels. First, it is required for compensation of higher losses in the path of vortex channel compared with that of Gaussian channel due to SPP and MO2, MO3. Moreover, as the experiments show, power in the Gaussian channel should be additionally reduced to some extent relative to the vortex channel in order to provide stable detection of both these spatial channels. This can be explained by different efficiency of beam coupling to the MEMS filters for Gaussian and OAM mode. The position of ATT1 is kept the same when receiving the Gaussian and OAM channels and their power difference after BS2 is kept at 1.45 dB throughout all the experiments.

For preliminary alignment of the SPP with the input IR beam, the fiber coupled red light laser is used, which points the SPP of proper azimuthal order on the wafer. For precise alignment of the SPPs, intensity distribution of its output beam is monitored using a phosphor-coated near IR CCD-camera, placed after BS2. Also the use of CCD-camera facilitates alignment of OAM-MUX in order to have Gaussian and vortex channels propagating parallel over the same spatial free space link. As the elements BS1, BS2, M1 and M2 form a Mach-Zehnder interferometer, it is convenient to control coincidence of Gaussian and vortex channels from the fringe patterns at the output of OAM-MUX – see the lower inset in Fig. 4. When aligning OAM-MUX, its feeding fiber is connected directly to the laser without modulators and WDM-MUX to have coherent radiation for contrast fringe patterns. The multiplexed signal is transmitted over a short (23 cm) free space link.

At the receiver side the multiplexed signal is focused by MO4, which matches the beam waist with the aperture of MEMS-filter, and incident to the SPP. The azimuthal order of SPP corresponds to the opposite topological charge of the vortex beam when receiving the OAM channel, and the MEMS-filter without SPP is used when receiving the Gaussian channel. Tuning of the filters is realized by controlling the substrate temperature with a thermoelectric cooler (TEC) element. MO5 provides collimation of the beam transmitted through the MEMS-filter, and MO6 provides coupling of this beam to the standard single mode fiber (SSMF), which serves as a spatial filter supporting only the Gaussian mode, and also as a link to the photo-detector. Mirrors M3, M4 provide alignment of the MEMS-filter output beam to

Optics EXPRESS

the fiber. It is worth noting, that physically the MEMS filter itself does not provide the OAM multiplexing, but rather shifts the OAM order by a value equal to the respective deposited SPP. All output OAM orders are coupled to the fiber, but only Gaussian one survives after several meters of propagation. Several methods have been suggested to simultaneously demultiplex different OAM orders, e.g. based on optical elements [24,25] or metasurface [31]. Detection of the received signal is provided by an avalanche photodiode (APD); in case when phase modulation is applied, delay line interferometer (DLI) is used before the APD.

4. Results

The experimental setup allows us to measure Bit Error Rate (BER) as a function of Received Optical Power (ROP) for different number of information channels in order to determine the penalties when simultaneous WDM and OAM multiplexing/demultiplexing is performed. Thus, four different cases in our proof-of-concept experiment have been considered: one channel (reference BER curve for one wavelength and each OAM alone), two spatial channels at the same wavelength but different OAMs, two wavelength channels without extra OAM multiplexing, and four channels where two spatial and two wavelength channels are combined, see Fig. 5. The series of BER measurements mentioned above is implemented in both the OAM channel and Gaussian channel, using for demultiplexing the filters with and without SPP respectively. During the measurements, the received channel has the wavelength in the range from 1536 to 1544 nm. We suppose the BER curves at other wavelengths should be similar over the vortex MEMS filters tuning range as the results of [34] and Fig. 2 suggest. The spacing between channels in wavelength domain is fixed and equals 0.8 nm.

In case of two transmitted OAM channels, the measured one is tagged as (Rx). For example, when two channels with $l = 0$ and $l = 1$ are being transmitted at the same wavelength, the sign $l(\mathrm{Rx}) = 0$ means that the Gaussian channel is measured, and the sign $l(\mathrm{Rx}) = 1$ denotes measuring of the OAM channel. This notation is assumed for all figures and tables.

In order to verify that OAM/wavelength multiplexing with proposed devices is transparent to modulation formats, the same sets of BER curves vs. Received Optical Power (ROP) have been collected for two basic optical modulation formats – On-Off Keying (OOK), see Fig. 5, left column, and Binary Phase Shift Keying (BPSK), see Fig. 5, right column. All complex modulation formats represent combinations of amplitude and phase modulations. In case of BPSK the power budget was limited at lower values (up to –27 dBm) because of losses in DLI. We do not use amplifiers at the receiver side in order to avoid the noise due to ASE. As a result, ROP limit does not allow us to demonstrate error-free transmission within our setup in case of BPSK, but the values of BER are lower compared with OOK at the same ROPs according to the theoretical predictions. Extrapolation of BER curves for higher ROPs in case of BPSK can show error-free transmission analogously to the demonstrated BER curves in case of OOK.

As defined in optical transmission network (OTN) standard, BER below 3.8×10^{-3} is required for successful transmission using Forward Error Correction (FEC) with 7% overhead (OH). However, this BER threshold seems not reasonable for the scenarios of short-reach optical links and data center interconnects because of large overhead and high latency of FEC. For example, the IEEE 802.3bm standard implies FEC with 2.7% OH Reed-Solomon (RS) code with 100 ns latency. This type of FEC requires BER threshold at 1.42×10^{-5} to achieve output BER lower than 10^{-15} [41,42]. Therefore, at the BER graphs for OOK modulation the BER limit at 1.42×10^{-5} is also considered.

Optics EXPRESS

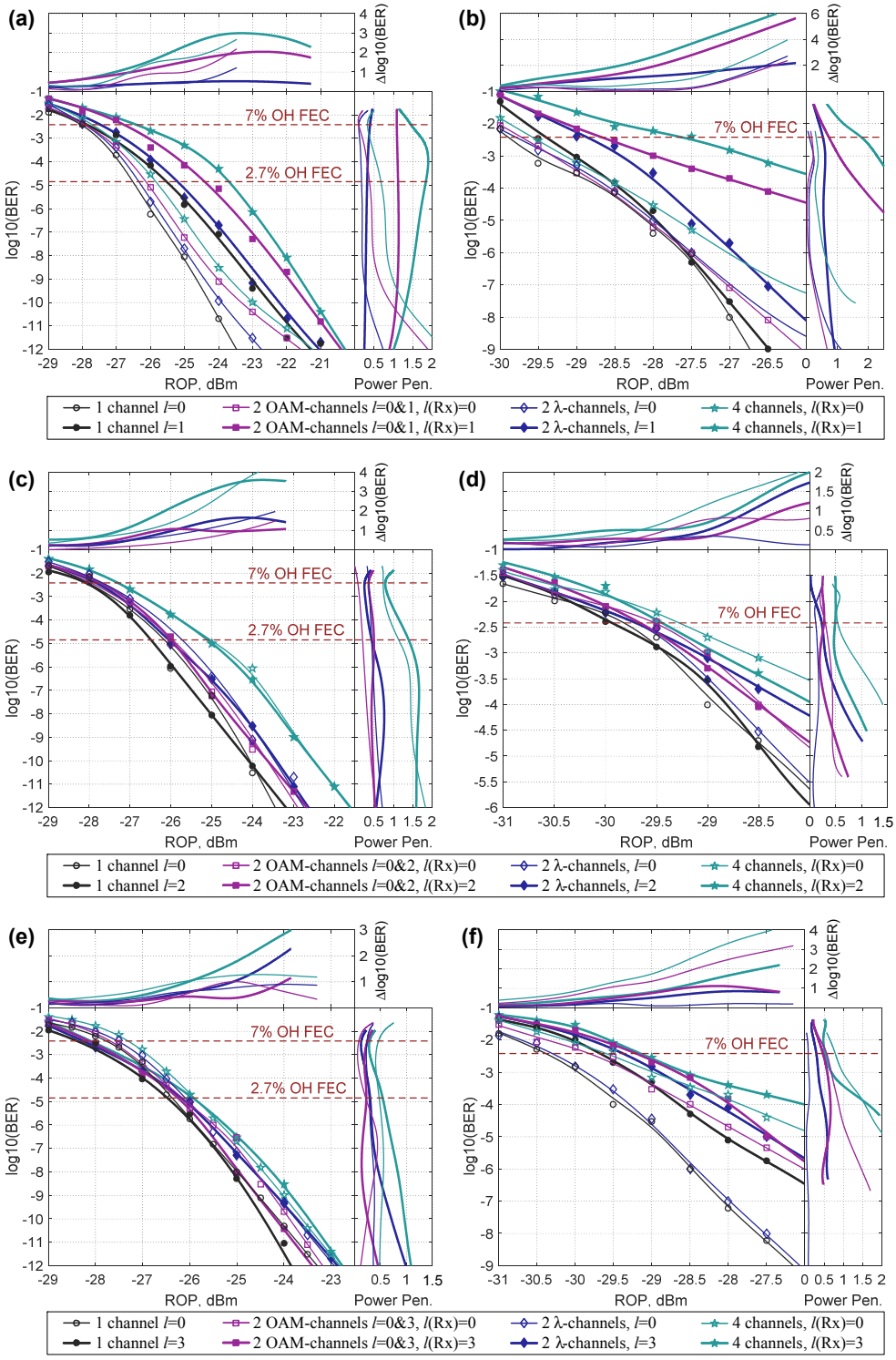

Fig. 5. BER vs. ROP curves and penalties for demultiplexing wavelength and OAM channels when transmitting the Gaussian channel and the OAM channel of order: (a),(b) l = 1; (c),(d) l = 2; and (e),(f) l = 3. The left column [(a),(c),(e)] corresponds to OOK modulation, and the right column [(b),(d),(f)] corresponds to BPSK modulation.

Optics EXPRESS

To assess the performance of transmission system when demultiplexing wavelength and OAM channels with our vortex MEMS filters, we calculate the ROP penalties at different BER levels. From Fig. 5 the general conclusion can be made that the closer azimuthal orders of the transmitted OAM channels, the higher BER and power penalties. The best results (lower penalties) appear in case of maximum OAM separation, namely with $l = 3$ and $l = 0$, and OOK modulation – see Fig. 5(e). For less OAM separation the BER and power penalties generally increase. Values of power penalties at the FEC BER thresholds for the case of four (two wavelength and two OAM) channels for OOK and BPSK are summarized in the Table 1.

Table 1. Penalties at the FEC BER thresholds for four (two OAM and two wavelength) channels, $\Delta\lambda = 0.8$ nm

Modulation		OOK		BPSK
BER threshold		7% OH HD-FEC	2.7% OH RS FEC	7% OH HD-FEC
l(Tx) = 0&1	l(Rx) = 0	0.33	0.68	0.32
	l(Rx) = 1	1.45	1.83	1.77
l(Tx) = 0&2	l(Rx) = 0	0.73	1.13	0.54
	l(Rx) = 2	0.79	1.39	0.49
l(Tx) = 0&3	l(Rx) = 0	0.46	0.47	0.79
	l(Rx) = 3	0.29	0.54	0.52

In order to assess the selectivity of the vortex MEMS filters in the wavelength domain, we measured performance of the system for different spacing $\Delta\lambda$ between wavelength channels in case of OOK modulation. Figure 6 shows the corresponding BER measurement results. The devices were tested for the case of simultaneous multiplexing of two wavelength and two OAM channels, and $\Delta\lambda$ was decreasing from 0.8 nm with the step of 0.1 nm while the wavelength channels remained separable. As before, values of BER in both the OAM channel and the Gaussian channel were measured. Penalties were calculated relative to the case of largest spacing $\Delta\lambda = 0.8$ nm.

As the MEMS filter proves to possess non-symmetric bandwidth at the resonance wavelength (with increasing the wavelength the transmittance increases smoothly up to the resonance and then falls down abruptly), two scenarios were tested: when the influencing channel has the lower and the higher wavelength relative to the received channel, see Fig. 6, left and right columns respectively. It is clearly seen that the MEMS-filter suppresses the non-resonant channel differently depending on the positioning of the suppressed channel.

The performance degradation due to crosstalk between wavelength channels becomes distinguishable for $\Delta\lambda \leq 0.5$ nm in the case when the received channel has higher wavelength than the filtered channel, and for $\Delta\lambda \leq 0.4$ nm when the received channel has lower wavelength than the filtered channel. But in the former case the received signal remains detectable with the BER values lower than 7% OH FEC threshold even with $\Delta\lambda = 0.2$ nm, while in the latter case the quality of the received signal degrades rapidly with diminishing the spacing between wavelength channels beyond 0.4 nm. Nevertheless, wavelength channels in the latter case still can be demultiplexed when $\Delta\lambda = 0.3$ nm. Therefore, the overall behavior of MEMS-filters in wavelength domain suggests its reasonable usage with the 50 GHz DWDM frequency grid [43]. Table 2 summarizes maximum ROP penalties (among both placement scenarios of wavelength channels mentioned above) when multiplexing the Gaussian beam and OAM beams of azimuthal orders $l = 1$, 2 and 3.

Optics EXPRESS

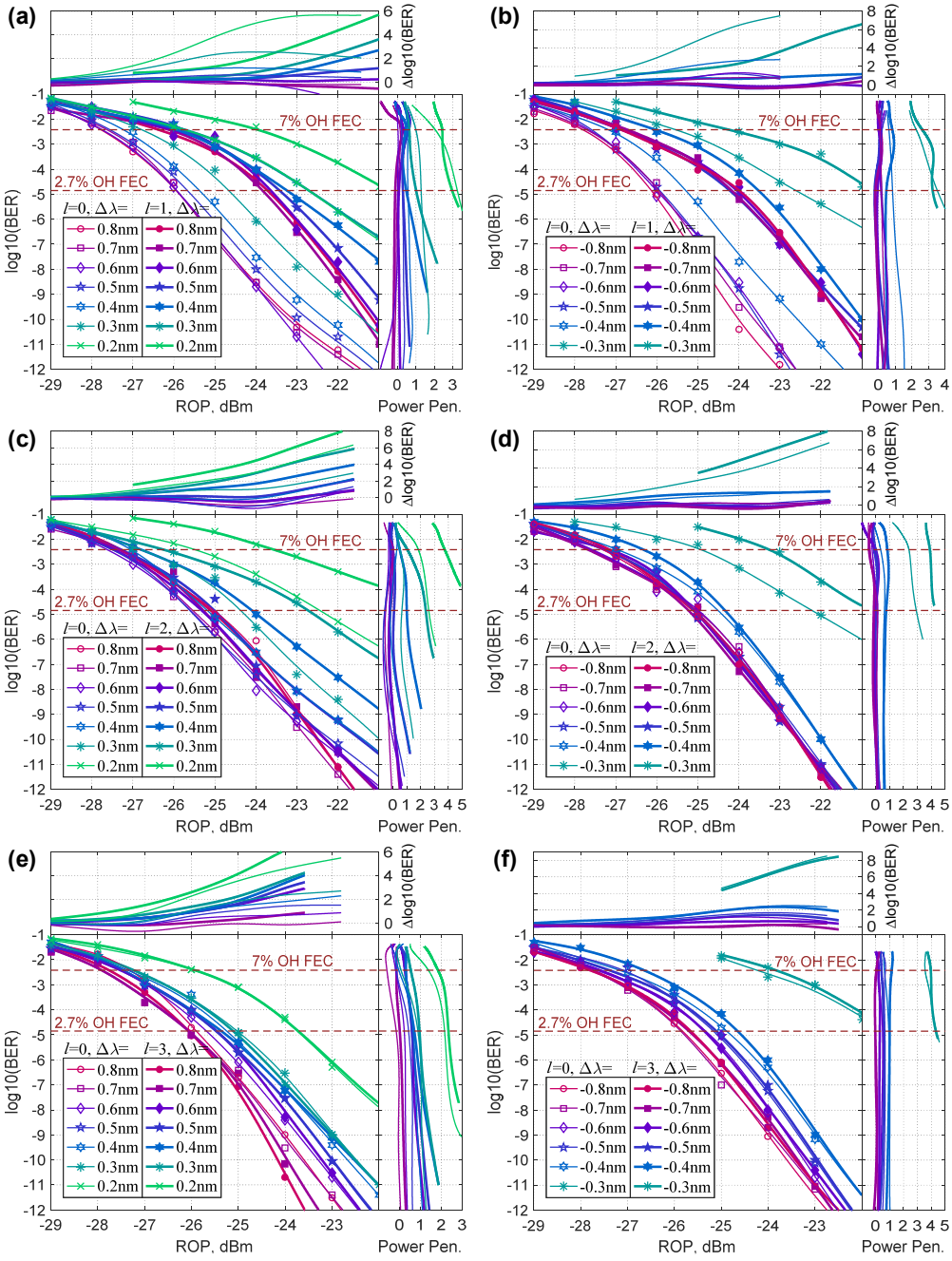

Fig. 6. BER vs. ROP curves and penalties for OOK modulation when four (two wavelength and two OAM) channels are being transmitted for different spacing between wavelength channels. Each graph corresponds to transmission of the Gaussian channel and the OAM channel of order: (a),(b) l = 1; (c),(d) l = 2; and (e),(f) l = 3. The left column [(a),(c),(e)] and the right column [(b),(d),(f)] correspond to the cases when the received channel has higher and lower wavelength, than the filtered channel, respectively.

Optics EXPRESS

Table 2. Maximum penalties at the FEC BER thresholds for multiplexing four channels, $\Delta\lambda$ = 0.4 nm relative to $\Delta\lambda$ = 0.8

BER threshold		7% OH HD-FEC	2.7% OH RS FEC
l(Tx) = 0&1	l(Rx) = 0	0.62	0.84
	l(Rx) = 1	0.83	0.48
l(Tx) = 0&2	l(Rx) = 0	0.35	0.63
	l(Rx) = 2	0.84	1.00
l(Tx) = 0&3	l(Rx) = 0	0.62	0.94
	l(Rx) = 3	1.15	1.00

Thus, from Figs. 5 and 6 the summarizing conclusion can be drawn, that the behavior of the vortex MEMS-filters in both wavelength and OAM domains is similar – the larger spacing between channels in each multiplexing domain the better the transmission system performance (lower BER and power penalties), and vice versa.

In order to fully characterize the functionality of the presented filter construction, it is necessary to make tests with more OAM channels. In this case an impact of their cross talk will be characterized closer to the real transmission conditions.

5. Conclusion

In this paper, we demonstrated a new wavelength-tunable micro-component for simultaneous selection of the waves with different wavelengths and values of OAM – MEMS-based Fabry-Perot filter with integrated spiral phase plate. The proposed device is suitable for dense on-chip integration and is dedicated for the next generation optical links in both long-haul and short-range scenarios, simultaneously utilizing all three degrees of freedom of the electromagnetic waves: wavelength, polarization, and OAM.

Experimental measurements of system performance when multiplexing two wavelength channels (with 0.8 nm spacing) and two OAM channels (Gaussian beam is combined with OAM beams of azimuthal orders l = 1, 2, 3) demonstrate, that in the case of intensity modulation penalties do not exceed 1.45 dB and 1.83 dB at the 7% and 2.7% OH FEC BER thresholds, respectively. With the ROP up to –20 dBm the error-free transmission (BER<10^{-12}) is demonstrated. In the case of phase modulation, penalties do not exceed 1.77 dB at the 7% OH FEC BER threshold.

Moderate penalties when shifting wavelength channels as close as 0.4 nm (1.15 dB and 1 dB at the abovementioned BER thresholds respectively) suggest usage of the proposed devices with the 50 GHz DWDM frequency grid. At the same time, transmission tests when multiplexing Gaussian beam with OAM beams of different orders demonstrate the behavior of the vortex MEMS filters in OAM domain generally similar to that in the wavelength domain – the larger the distance between multiplexed channels, the better the transmission system performance.

Funding

Helmholtz Program Science and Technology of Nanosystems (STN); Karlsruhe School of Optics and Photonics (KSOP); KIT Nanostructure Service Laboratory (NSL); Russian Fund for Basic Research (RFBR) (16-47-630546, 16-47-630677).

Acknowledgments

Authors acknowledge Yannick Hopf and Felix Lenze for their contribution to the experimental setup.

129.13.72.197 (ts 2018-11-16 03:28:33)